Two-Dimensional Dynamical Jahn–Teller Effects in a Mixed-Valence Benzotriazolato Copper Cluster, $Cu_5(BTA)_6(RNC)_4$

G. F. Kokoszka,*[1a] J. Baranowski,[1a,b] C. Goldstein,[1a] J. Orsini,[1a] A. D. Mighell,*[1c] V. L. Himes,[1c] and A. R. Siedle*[1d]

Contribution from the Department of Chemistry, State University of New York, Plattsburg, New York 12901, Center for Materials Science, National Bureau of Standards, Washington, D.C. 20234, Department of Chemistry, The Catholic University of America, Washington, D.C. 20064, and Science Research Laboratory, 3M Central Research Laboratories, St. Paul, Minnesota 55101. *Received November 1, 1982*

Abstract: Clusters of composition $Cu_5(BTA)_6(RNC)_4$ [BTA = benzotriazolato(1−)] were prepared from the reaction of copper(I) thiophenoxide, benzotriazole, and an organic isocyanide. $Cu_5(BTA)_6(t\text{-}C_4H_9NC)_4$ crystallizes in space group $P\bar{4}2_1c$, a = 13.836 (4) Å, c = 16.686 (4) Å, Z = 2, D_{calcd} = 1.413, D_{obsd} = 1.41 (2) Mg m^{-3}. The structure solution, based on 903 reflections, converged at R = 0.063 and R_w = 0.047. The molecular structure has $\bar{4}$ symmetry; compressed octahedral copper(II) is surrounded by four tetrahedrally coordinated copper(I) ions. η_3-Benzotriazolato(1−) ligands connect each Cu(I) ion with three symmetry-related Cu(I) sites and with the central Cu(II). Terminal t-C_4H_9NC ligands are bonded to Cu(I). EPR data were obtained at various temperatures in the liquid nitrogen to room temperature range. Data were recorded at 9, 24, and 54 GHz. The large Cu(II)–Cu(II) distance of 12.858 Å in this cluster ensures that the effects of exchange interactions are virtually nonexistent and that electronic dipolar broadening would be small. The appearance of Cu(II) hyperfine structure in almost all of the spectra supports this expectation. Furthermore, the EPR data are not consistent with a d_{z^2} ground state in spite of the compressed octahedral molecular geometry. At low temperatures, the EPR spectra are quite normal: $g_\parallel$ = 2.271 (4), $g_\perp$ = 2.069 (4), $A_\parallel$ = (145 ± 4) × 10^{-4} cm^{-1}, and $A_\perp$ = 0, consistent with a $d_{x^2-y^2}$-type ground state. Above 128 K, a "reversed spectrum" is observed and is interpreted in terms of a two-dimensional dynamical Jahn–Teller effect. The other three compounds also showed interesting temperature-dependent effects.

Introduction

EPR studies of the Jahn–Teller effect[2-5] can usually be placed in one of two major categories. The first type involves the doping of the paramagnetic ion into a diamagnetic host lattice in low concentrations in order to achieve magnetic isolation and thereby provide a wealth of fine and hyperfine structural information. On the other hand, this information may be obtained only at the cost of imperfect information about the local geometry of the paramagnetic probe.[6] The second category includes studies of pure materials that may be structurally well characterized but suffer from a lack of magnetic dilution and frequently exhibit exchange averaging effects or cooperative phenomena. In this paper we investigate, by X-ray crystallographic and EPR methods, a new class of clusters discovered in the course of our research on the coordination chemistry of benzotriazole,[7-11] a corrosion inhibitor for copper and its alloys. They are structurally well defined at room temperature and exhibit a dynamical Jahn–Teller effect with certain unique features that have not previously been reported. These materials are the mixed-valence clusters $Cu_5(BTA)_6(RNC)_4$ [R = alkyl, aryl; BTA = benzotriazolato(−1)]. A preliminary report of some structural information on **1** (R = t-C_4H_9) has appeared.[11] In addition to the complex with a *tert*-butylisocyanide ligand coordinated to each of the four Cu(I) cations, three related materials, **2** (R = c-C_6H_{11}), **3** (R = i-C_3H_7), and **4** (R = C_6H_5), have also been studied by EPR methods and provide striking evidence of the sensitivity of this technique to molecular variations that, at first sight, appear to be quite small. We begin by considering in more detail the molecular structure of **1**.

Experimental Section

The copper benzotriazole clusters reported in this paper were prepared by combining copper(I) thiophenoxide, benzotriazole, and an isocyanide in dichloromethane. The synthesis of $Cu_5(BTA)_6(t\text{-}C_4H_9NC)_4$ (**1**) below is exemplary.

In a 50-mL flask that had been flushed with nitrogen were placed 1.72 g (10 mmol) of powdered copper(I) thiophenoxide (Alfa), 1.43 g (12 mmol) of benzotriazole, and 25 mL of dichloromethane. *tert*-Butylisocyanide, 0.8 mL, was added through a rubber septum. After stirring for 15 min, the reaction mixture was filtered in air to provide 0.55 g (20%) of **1** as an orange powder, which was washed with fresh solvent and vacuum-dried. The filtrate was transferred to a stoppered flask and allowed to stand undisturbed for several days. Small orange crystals of **1** slowly formed. These were isolated by filtration and used for subsequent X-ray studies. The infrared spectra of the polycrystalline product and the crystals used for the structure determination were identical.

1: Anal. Calcd for $C_{56}H_{60}Cu_5N_{22}$: C, 49.5; H, 4.4; N, 22.7. Found: C, 49.3; H, 4.4; N, 22.7. IR (KBr) 3060 (w), 2980 (m), 2930 (w), 2140 (s), 1450 (m), 1395 (m), 1370 (m), 1200 (s), 1170 (s), 990 (w), 785 (m), 750 (s), 740 (s), 640 (w), 280 (m) cm^{-1}.

2: Anal. Calcd for $C_{64}H_{68}Cu_5N_{22}$: C, 52.5; H, 4.6; Cu, 21.9; N, 21.0. Found: C, 52.7; H, 4.8; Cu, 21.9; N, 21.1. IR (KBr) 3060 (w), 2940 (s), 2860 (m), 2140 (s), 1450 (s), 1395 (m), 1365 (m), 1325 (m), 1270 (w), 1170 (s), 1130 (w), 990 (m), 790 (m), 745 (s), 690 (m), 640 (w), 555 (w), 430 (w), 275 (m) cm^{-1}.

3: Anal. Calcd for $C_{52}H_{52}Cu_5N_{22}$: C, 48.0; H, 4.0; N, 23.7. Found: C, 47.6; H, 4.0; N, 23.7. IR (Nujol) 2140 (s), 1490 (m), 1445 (s), 1375 (m), 1335 (s), 1305 (w), 1215 (w), 1190 (s), 1180 (s), 1165 (s), 1120 (s), 990 (m), 785 (m), 740 (s), 690 (m), 635 (w), 555 (w), 430 (w), 370 (w), 225 (m) cm^{-1}.

4: Anal. Calcd for $C_{64}H_{44}Cu_5N_{22}$: C, 53.4; H, 3.1; N, 21.4. Found: C, 53.5; H, 3.0; N, 21.1. IR (Nujol) 2120 (s), 1580 (w), 1485 (m), 1445 (s), 1370 (m), 965 (s), 790 (m), 740 (s), 690 (w), 680 (m), 550 (w), 540 (w), 500 (w), 430 (w) cm^{-1}.

Crystal Structure Determination. The complex $Cu_5(BTA)_6(t\text{-}C_4H_9NC)_4$ crystallizes in the tetragonal crystal system, space group $P\bar{4}2_1c$

(1) (a) State University of New York. (b) Permanent address: Institute of Chemistry, Wroclaw University, Wroclaw, Poland. (c) National Bureau of Standards. (d) 3M Central Research Laboratories.
(2) D. Reinen and C. Friebel, *Struct. Bond. (Berlin)* **37**, 1 (1979).
(3) I. B. Bersuker, *Coord. Chem. Rev.*, **14**, 357 (1975); J. Gazo, I. B. Bersuker, J. Garaj, M. Kabesova, J. Kohout, H. Langfelderova, M-Melnik, M. Serator, and F. Valach, *ibid.*, **19**, 253 (1976).
(4) R. Engleman, "The Jahn–Teller Effect in Molecules and Crystals", Wiley-Interscience, New York, 1971.
(5) J. H. Ammeter, H. B. Burgi, E. Gamp, V. Meyer-Sandrin, and W. P. Jensen, *Inorg. Chem.*, **18**, 733 (1979).
(6) J. Azoulay, E. A. Stern, D. Shaltiel, and A. Grayevski, *Phys. Rev. B*, **25**, 5627 (1982).
(7) A. R. Siedle, R. A. Velapoldi, and N. E. Erickson, *Inorg. Nucl. Chem. Lett.*, **15**, 33 (1979).
(8) A. R. Siedle, R. A. Velapoldi, and N. E. Erickson, *Appl. Surf. Sci.*, **3**, 229 (1979).
(9) J. Reedijk, G. Roelofsen, A. R. Siedle, and A. L. Spek, *Inorg. Chem.*, **18**, 1947 (1979).
(10) L. D. Brown, J. A. Ibers, and A. R. Siedle, *Inorg. Chem.*, **17**, 3026 (1978).
(11) V. L. Himes, A. D. Mighell, and A. R. Siedle, *J. Am. Chem. Soc.*, **103**, 211 (1981).

0002-7863/83/1505-5627$01.50/0

Table I. Positional Parameters with Estimated Standard Deviations in Parentheses

atom	x	y	z
Cu2	0.5	0.5	0.5
Cu1	0.41452 (15)	0.29876 (14)	0.37886 (11)
N1	0.3498 (10)	0.4394 (10)	0.5003 (8)
N2	0.2796 (10)	0.4720 (9)	0.5463 (7)
N3	0.3220 (11)	0.3585 (10)	0.4577 (7)
N4	0.5	0.5	0.3750 (9)
N5	0.4646 (8)	0.4300 (9)	0.3331 (6)
N6	0.3465 (11)	0.1539 (11)	0.2554 (9)
C1	0.2028 (14)	0.4138 (13)	0.5346 (8)
C2	0.1080 (15)	0.4120 (16)	0.5654 (10)
C3	0.0419 (15)	0.3452 (18)	0.5426 (13)
C4	0.0724 (19)	0.2773 (16)	0.4865 (16)
C5	0.1638 (17)	0.2706 (14)	0.4534 (12)
C6	0.2292 (14)	0.3423 (13)	0.4790 (10)
C7	0.4778 (15)	0.4547 (9)	0.2550 (7)
C8	0.4531 (13)	0.4076 (11)	0.1840 (8)
C9	0.4761 (17)	0.4552 (10)	0.1148 (8)
C10	0.3728 (11)	0.2059 (13)	0.3041 (10)
C11	0.3104 (19)	0.0922 (17)	0.1915 (13)
C12	0.2148 (24)	0.1270 (23)	0.1757 (18)
C13	0.2958 (24)	−0.0064 (18)	0.2225 (13)
C14	0.3690 (21)	0.1096 (23)	0.1236 (15)
H2	0.0873	0.4599	0.6070
H3	−0.0255	0.3424	0.5649
H4	0.0249	0.2284	0.4666
H5	0.1822	0.2177	0.4143
H8	0.4206	0.3423	0.1837
H9	0.4558	0.4257	0.0627

(No. 114), a = 13.836 (4) Å, c = 16.686 (4) Å, Z = 2, D_{calcd} = 1.413, D_{obsd} = 1.41 (2) Mg m^{-3} (flotation). Data were collected on a red-orange crystal of dimensions of 0.10 × 0.11 × 0.11 mm by using an automated four-circle diffractometer with graphite monochromated Mo Kα radiation, λ = 0.71069 Å. The cell dimensions were determined by a least-squares refinement of setting angles of 15 reflections with 2θ values ranging between 15 and 25°. Systematic extinctions observed on the diffractometer established the space group as $P\bar{4}2_1c$. Integrated diffraction intensities were measured in the bisecting mode with $3.0 \le 2\theta \le 45.0°$. The peaks were scanned over a range of $2\theta(K\alpha_1) - 0.8°$ to $2\theta(K\alpha_2) + 1.0°$ by using variable scan rates of 2.0–29.3° min^{-1} depending on the intensity of the preliminary count. Background counts were taken at each end of the scan with a ratio of total background time to scan time of 0.5. Four standard reflections that were measured periodically showed no apparent decrease in intensity during data collection. The estimated standard deviation in intensity $\sigma(I)$ was calculated from $\sigma(I)^2 = TC + 0.000491(TC)^2$, where TC is the total observed counts and the constant was derived from a statistical analysis of the intensity distributions of the four standard reflections. The data were corrected for Lorentz and polarization effects. In view of the crystal size and linear absorption coefficient (μ = 16.9 cm^{-1}), no absorption correction was applied. Of the 1196 unique reflections measured, 903 had $F_o \ge 3\sigma(F_o)$ and were subsequently used for structure determination and refinement.

The positions of the two independent copper atoms were determined by direct methods using MULTAN.[12] Successive Fourier syntheses revealed the positions of the remaining non-hydrogen atoms. In the final anisotropic refinement, the hydrogen atoms on the benzene moieties were held fixed in calculated positions (trigonal geometry, C–H = 1.0 Å) each with an isotropic U of 0.08 Å^2. Due to the apparent disorder of the methyl groups in the *tert*-butylisocyanide ligand, the methyl hydrogen atoms were not included in the refinement. The final cycle of full-matrix least-squares anisotropic refinement resulted in an R ($=\sum||F_o| - |F_c||/\sum|F_o|$) of 0.063 and R_w ($=\sum w^{1/2}||F_o| - |F_c||/\sum w^{1/2}F_o$) of 0.047. The function minimized was $\sum w(|F_o| - |F_c|)^2$, where $w = [\sigma(F_o)]^{-2}$. Analysis of the final difference map revealed no peak greater than 0.54 e Å^{-3}. The scattering factors used were those of Cromer and Mann[13] for C, Cu, and N and that of Stewart et al.[14] for H. Corrections for anomalous dispersion were applied for copper ($\Delta f'$ = 0.263, $\Delta f''$ = 1.266).[15]

Table II. Selected Interatomic Distances (Å) and Angles (deg) for 1 with Estimated Standard Deviations in Parentheses[a]

Cu2···Cu1	3.638 (2)	N2–C1	1.35 (2)
Cu2–N1	2.241 (13)	N3–C6	1.35 (2)
Cu2–N4	2.085 (16)	N4···N1b	3.058 (17)
Cu1···Cu1b	5.886 (3)	N4–N5	1.292 (14)
Cu1···Cu1c	6.050 (3)	N5–C7	1.360 (16)
Cu1···N1	2.949 (13)	C1–C2	1.41 (3)
Cu1···N1b	2.941 (13)	C1–C6	1.40 (2)
Cu1–N2b	2.024 (12)	C2–C3	1.35 (3)
Cu1–N3	2.013 (14)	C3–C4	1.39 (3)
Cu1···N4	3.026 (2)	C4–C5	1.38 (3)
Cu1–N5	2.087 (12)	C5–C6	1.41 (3)
Cu1–C10	1.882 (17)	C7–C7c	1.40 (2)
N1···N1b	3.169 (19)	C7–C8	1.40 (2)
N1–N2	1.318 (19)	C8–C9	1.37 (2)
N1–N3	1.381 (19)	C9–C9c	1.40 (2)
N1···N4	3.064 (17)		
Cu1···Cu2···Cu1b	107.98 (5)	N1–N2–C1	107.0 (12)
Cu1···Cu2···Cu1c	112.50 (5)	N1–N3–C6	105.3 (13)
N1–Cu2–N1b	90.0 (5)	Cu2–N4–N5	122.8 (8)
N1–Cu2–N1c	179.8 (5)	Cu1···N4···Cu1c	177.6 (6)
N1–Cu2–N4	90.1 (3)	N1···N4···N1b	62.3 (4)
N1b–Cu2–N4	89.9 (3)	N5–N4–N5c	114.4 (13)
Cu1b···Cu1···Cu1c	59.07 (3)	Cu1–N5–N4	125.5 (9)
Cu1b···Cu1···Cu1d	61.85 (4)	Cu1–N5–C7	127.9 (9)
N1···Cu1···N1b	65.1 (4)	N4–N5–C7	106.2 (12)
N1···Cu1···N4	61.7 (4)	N2–C1–C2	133.8 (16)
N1b···Cu1···N4	61.6 (3)	N2–C1–C6	108.2 (15)
N2b–Cu1–N3	98.3 (5)	C2–C1–C6	118.1 (17)
N2b–Cu1–N5	94.7 (5)	C1–C2–C3	122.5 (18)
N2b–Cu1–C10	123.9 (7)	C2–C3–C4	116.4 (20)
N3–Cu1–N5	95.3 (5)	C3–C4–C5	126.3 (22)
N3–Cu1–C10	121.2 (6)	C4–C5–C6	114.7 (18)
N5–Cu1–C10	117.0 (6)	N3–C6–C1	107.7 (16)
Cu2–N1–N2	123.8 (10)	N3–C6–C5	130.3 (17)
Cu2–N1–N3	124.1 (10)	C1–C6–C5	122.0 (18)
Cu1···N1···Cu1d	176.0 (5)	N5–C7–C7c	106.6 (11)
N1b···N1···N1d	90.0 (5)	N5–C7–C8	131.5 (14)
N1b···N1···N4	58.7 (4)	C7c–C7–C8	121.9 (12)
N1d···N1···N4b	58.9 (4)	C7–C8–C9	115.7 (14)
N2–N1–N3	111.8 (12)	C8–C9–C9c	122.4 (13)
Cu1d–N2–N1	121.9 (10)	Cu1–C10–N6	175.8 (16)
Cu1d–N2–C1	131.0 (11)		

[a] The letters a–d refer to the following equivalent positions: a (no symbol) = x, y, z; b = $1-y, x, 1-z$; c = $1-x, 1-y, z$; d = $y, 1-x, 1-z$.

All calculations (except MULTAN) were performed with the X-Ray System.[16] The program ORTEP[17] was used in the preparation of the figures. Table I lists the final positional parameters; Table II lists selected interatomic distances and angles.

The EPR data for $Cu_5(BTA)_6(t\text{-}C_4H_9NC)_4$ were collected in the temperature range 77–300 K at X-band frequency with a Varian spectrometer system and a Varian variable-temperature gas-flow apparatus as well as with low-temperature slushes in an insert Dewar. In addition, data were obtained at K-band and V-band frequencies at room temperature and liquid nitrogen temperature by using reflection spectrometers constructed at Plattsburgh. The latter employed 275-Hz magnetic field modulation, single-ended crystal detectors, and a PAR lock-in amplifier. At X-band, the Varian multipurpose cavity and a brass cylindric cavity were used with the Varian 100-KHz modulation unit. At K-band and V-band, the sample was placed directly in a section of shortened wave guide, and no cavity was employed. In this way artificial line broadening due to overloading was avoided. The amount of samples placed in the shortened wave guide could be about 2 orders of magnitude greater than that which might be used in a cavity system. This nearly compensates for the decreased sensitivity due to the loss of the multiplicative cavity Q factor.

The other three samples were studied less extensively but under essentially the same circumstances as described above. Most data were obtained with a Varian field dial as the calibration device, but selected

(12) G. Germain, P. Main, and M. M. Woolfson, *Acta Crystallogr., Sect. A*, **27A**, 368 (1971).
(13) D. T. Cromer and J. B. Mann, *Acta Crystallogr., Sect. A*, **24A**, 321 (1968).
(14) R. F. Stewart, E. R. Davidson, and W. T. Simpson, *J. Chem. Phys.*, **42**, 3175 (1965).
(15) "International Tables for X-ray Crystallography", Vol. IV, Kynoch Press, Birmingham, England, 1974, p 149.
(16) J. M. Stewart, P. A. Machin, C. W. Dickinson, H. L. Ammon, H. Heck, and H. Flack, XRAY76, Technical Report TR-446, Computer Science Center, University of Maryland, College Park, MD.
(17) C. K. Johnson, ORTEP, Report ORNL-3794, Oak Ridge National Laboratory, Oak Ridge, TN, 1965.

Table III. Selected Interplanar Angles (deg)

	eq BTA				ax BTA		plane 1[c] (Cu2		
	a[a]	b	c	d	a, c[b]	b, d	basal plane)	plane 2[d]	plane 3[e]
eq BTA a		56.2	83.5	56.2	57.4	66.9	41.7	48.5	86.6
eq BTA b	56.2		56.2	83.5	66.9	57.4	41.7	86.6	48.5
eq BTA c	83.5	56.2		56.2	57.4	66.9	41.7	48.5	86.6
eq BTA d	56.2	83.5	56.2		66.9	57.4	41.7	86.6	48.5
ax BTA a, c	57.4	66.9	57.4	66.9		90.0	90.0	41.1	48.9
ax BTA b, d	66.9	57.4	66.9	57.4	90.0		90.0	48.9	41.1
plane 1 (Cu2 basal plane)	41.7	41.7	41.7	41.7	90.0	90.0		90.0	90.0
plane 2	48.5	86.6	48.5	86.6	41.1	48.9	90.0		90.0
plane 3	86.6	48.5	86.6	48.5	48.9	41.1	90.0	90.0	

[a] Symmetry codes a-d are defined in Table II; atoms defining equatorial BTA a are N1a, N2a, N3a, C1a, C2a, C3a, C4a, C5a, C6a. [b] Atoms defining axial BTA a, c are N4a, N5a, N5c, C7a, C7c, C8a, C8c, C9a, C9c. [c] Atoms defining plane 1 are Cu2, N1a, N1b, N1c, N1d. [d] Atoms defining plane 2 are Cu2, N1a, N1c, N4a, N4b. [e] Atoms defining plane 3 are Cu2, N1b, N1d, N4a, N4b.

Table IV. EPR Data

compound	T, K	$g_\parallel$	$g_\perp$	$A_\perp$, $cm^{-1} \times 10^{-4}$	$A_\parallel$, $cm^{-1} \times 10^{-4}$
$Cu_5(BTA)_6(t\text{-}C_4H_9NC)_4$, 1	>128	2.069 (4)	2.177 (4)	68 (4)	
	<128	2.271 (4)	2.069 (4)		145 (4)
$Cu_5(BTA)_6(c\text{-}C_6H_{11}NC)_4$, 2	>210	2.082 (4)	2.168 (4)	56 (4)	
	<210	2.289 (4)	2.077 (4)		127 (4)
$Cu_5(BTA)_6(i\text{-}C_3H_7NC)_4$, 3	>290	2.17 (1)	2.17 (1)	48 (5)	
	<100	2.298 (5)	2.080 (5)		163 (4)
$Cu_5(BTA)_6(C_6H_5NC)_4$, 4	100	2.089 (4)	2.167 (5)	*a*	
		2.228 (4)	2.073 (4)		144 (4)

[a] Hyperfine structure not resolved.

spectra were recorded with an NMR gaussmeter used to monitor the magnetic field. At V-band, an external standard (single-crystal $CaCu(acetate)_4 \cdot 6H_2O$) was employed to calibrate the field and check the field dial. The g values for the latter material were taken to be $g_\parallel = 2.368$ and $g_\perp = 2.070$ at 295 K and $g_\parallel = 2.352$ and $g_\perp = 2.065$ at 77 K.[18] With only slight modification in design, the finger Dewar employed as an insert Dewar at X-band and 77 K could be used as an external Dewar for the shortened V-band wave guide section containing the sample. Table IV lists the EPR parameters. The uncertainties listed in parentheses are the maximum estimated values.

Description of the Structure

The crystal structure of $Cu_5(BTA)_6(t\text{-}C_4H_9NC)_4$ consists of neutral complexes with crystallographic $\bar{4}$ symmetry in which an octahedrally coordinated copper(II) ion is surrounded by four tetrahedrally coordinated copper(I) ions. Tridentate benzotriazolate ligands bridge each copper(I) ion to three symmetry-related copper(I) ions and to the central copper(II) ion. Figure 1 gives a view of the complex down a $\bar{4}$ axis. A stereoview of the complex is illustrated in Figure 2, and the labeling scheme is presented in Figure 3.

There are two complexes in the unit cell with the central Cu2 ions in special positions (0,0,0) and ($^1/_2$,$^1/_2$,$^1/_2$) with $\bar{4}$ symmetry. Each Cu2 ion is coordinated to four equatorial and two axial BTA ligands at the N1 and N4 positions, respectively. The four Cu1 ions surrounding the central Cu2 ion are each coordinated to one *tert*-butylisocyanide ligand and to three different BTA ligands (two equatorial and one axial) at the N2, N3, and N5 positions. The four equatorial BTA ligands illustrated in Figure 1 occupy general positions in the unit cell; within experimental error, their central nitrogen atoms (N1 positions) are in the $z = {}^1/_2$ plane ($z = 0$ plane for the complex at the origin) and are coplanar with Cu2. Because N4 lies on a crystallographic $\bar{4}$ axis, a 2-fold axis relates the two halves of the axial BTA ligands. Table III lists the angles formed between the planes of the BTA ligands and the three planes defined by Cu2 and the central nitrogen atoms of four BTA ligands.

The nature of the bridging between the copper ions is such that a three-dimensional copper–nitrogen cluster is formed in the center of the complex. As a tridentate ligand, BTA is involved in two types of copper–nitrogen–copper bridges. Bridging between Cu2 and Cu1 is accomplished via the central and an adjacent nitrogen atom of a BTA ligand. The four symmetry-related Cu1 ions are bridged by the two nitrogen atoms adjacent to the central nitrogen of a BTA ligand. The axial BTA ligands bridge two Cu1 ions situated on the same side of the Cu2 basal plane (i.e., the plane defined by Cu2 and the four N1 atoms) while the equatorial BTA ligands bridge Cu1 ions on opposite sides of the Cu2 basal plane. Thus, the central cluster is composed of interconnected copper–nitrogen cycles (azametallocycles) which vary in size and spatial orientation.

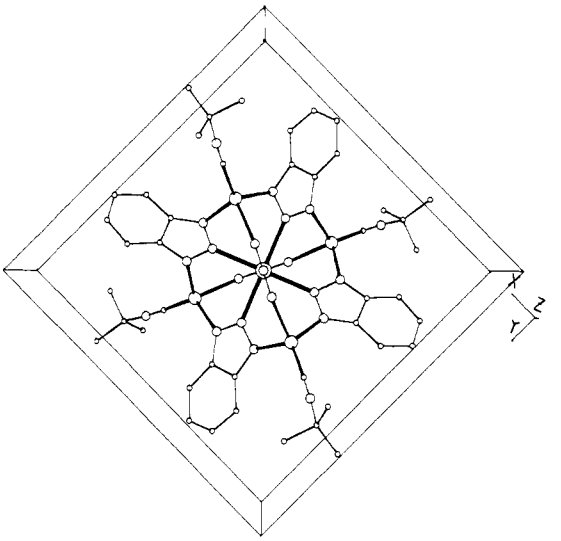

Figure 1. Structure of $Cu_5(BTA)_6(t\text{-}C_4H_9NC)_4$ viewed down a crystallographic $\bar{4}$ axis (parallel to the z axis of the unit cell). For clarity, the benzene moieties of the axially coordinated BTA ligands, as well as the entire complex at the origin, have been omitted.

The geometry about Cu2 is unusual in that it is a compressed octahedron [(Cu2)(N1)$_4$(N4)$_2$]. In addition, because the four symmetry-related Cu1 ions lie 2.02 Å alternately above and below the Cu2 basal plane, a copper(I) tetrahedron [(Cu2)(Cu1)$_4$] is formed about Cu2. Thus, the core of the copper–nitrogen cluster

(18) J. A. Van Sauten, Thesis, Rijksuniversiteit Leiden, 1978, p 62.

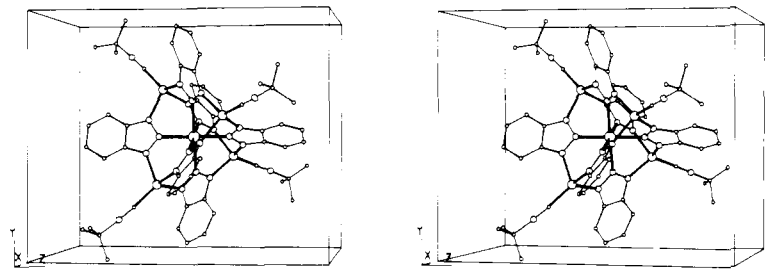

Figure 2. Stereoview of the complex viewed approximately down the x axis (10° rotation about y).

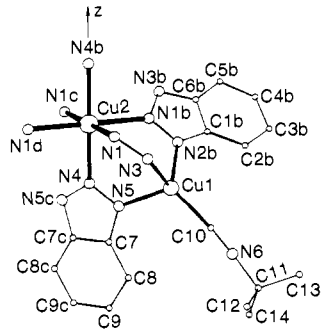

Figure 3. Perspective drawing showing the labeling scheme used. Unique atoms are labeled with atom type and number while the letters b–d refer to the equivalent positions defined in Table II.

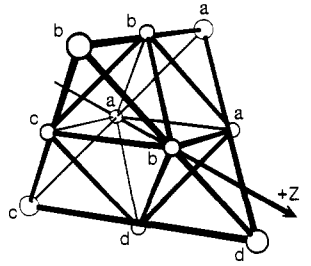

Figure 4. Geometric drawing showing that the core of the copper–nitrogen cluster may be viewed as a $(Cu2)(Cu1)_4$ tetrahedron with an inscribed $(Cu2)(N1)_4(N4)_2$ octahedron. The central Cu2 ion has not been drawn; the two N4 atoms lie along the z axis. The equivalent positions a–d are defined in Table II.

consists of an octahedron that is inscribed in a tetrahedron (Figure 4). The nitrogen atoms at the vertices of the octahedron lie very close to the midpoints of the edges of the circumscribed tetrahedron; each of the central nitrogen atoms of the BTA ligands are close to one copper(II) and two copper(I) ions (see Table II).

The complex $Cu_5(BTA)_6(t\text{-}C_4H_9NC)_4$ is slightly distorted from ideal cubic symmetry ($\bar{4}3m$) because of the chemical nature of the bonding to the central copper(II) ion. The stereochemistry about Cu2 is an undistorted octahedron of a compressed form with two axial Cu2–N4 bonds of 2.08 (2) Å and four symmetry-equivalent Cu2–N1 bonds of 2.24 (1) Å. This axial compression (parallel to the z axis of the unit cell) explains the slight distortion of the $(Cu2)(Cu1)_4$ tetrahedron. The two Cu1–Cu2–Cu1 angles along the line of compression are 112.50 (5)° while the other four angles are 107.98 (5)°. The two edges of the $(Cu2)(Cu1)_4$ tetrahedron normal to the line of compression are 6.050 (3) Å while the remaining four edges are 5.886 (3) Å.

EPR Spectra

The classification scheme for octahedral Jahn–Teller complexes outlined by Ammeter, Burgi, and co-workers[5] provides a useful framework for a discussion of some features of the studies reported here. To briefly summarize: Class I complexes include hexacoordinate Cu(II) ions occupying cubic or trigonal sites in "hard" lattice. These are often studied in dilute systems (e.g., Cu(II) in MgO)[19] since magnetically concentrated species often exhibit cooperative Jahn–Teller effects. The isolated cluster model is usually difficult to apply since the vibronic effects may be more characteristic of the host compound and, in any event, are associated with the continuous lattice.[5]

In class II, the paramagnetic site is generally only weakly coupled to other Jahn–Teller centers, and the cluster model should be applicable. Furthermore, these characteristics imply a certain degree of transferability of potential energy parameters among related complexes.[5] The Cu(II)–Cu(I) clusters should exhibit some of the features of class II complexes although they are of compressed octahedral symmetry. In particular, the transferability of potential energy parameters might have been expected to apply to the four complexes discussed in this paper. However, this is only approximately the case, and the details will be discussed below.

We next focus on some experimental aspects of EPR spectroscopy that are provided by the unique structural features of the $Cu_5(BTA)_6(RNC)_4$ clusters. First, essentially complete isolation of the paramagnetic centers from each other with a Cu(II)–Cu(II) distance between neighboring clusters of 12.858 Å in **1** results in the resolution of the Cu hyperfine structure. This isolation also reduces the exchange field between Cu(II) centers and the attendant possibility for exchange-averaging of EPR parameters and also reduces exchange-induced structural phase transitions.[2-5] Second, the change in the hyperfine pattern as a function of temperature as well as the line-width dependence on M_I is a significant aspect of the EPR data. Third, the frequency dependence of the appearance of the spectra of the polycrystalline samples provides examples of how the "parallel" and "perpendicular" portions of the EPR may alter in appearance.

A considerable amount of information is presently available concerning the structural and spectroscopic properties of six-coordinate Cu(II) complexes. The local site geometry is almost always tetragonally elongated. This elongation produces characteristic EPR parameters that are associated with $d_{x^2-y^2}$ ground state. In other molecules, polydentate ligands with relatively rigid skeletons may impose other geometrical microsymmetries at the Cu(II) site. In such cases, vibronic coupling effects often allow the $d_{x^2-y^2}$ level to become the ground state, at least at low temperature. These characteristics may be referred to as static and dynamic Jahn–Teller effects. In $Cu_5(BTA)_6(t\text{-}C_4H_9NC)_4$, the compressed octahedral geometry would seem to favor a d_{z^2} ground state. However, the EPR data presented below show a typical pattern associated with $d_{x^2-y^2}$ ground state near 77 K and peculiar behavior at higher temperature, which may be associated with a breakdown of the Born–Oppenheimer approximation leading to a dynamical two-dimensional Jahn–Teller effect.

Figure 5 presents temperature-dependent X-band EPR spectra of $Cu_5(BTA)_6(t\text{-}C_4H_9NC)_4$. The lower curve shows the major features associated at 77 K with typical polycrystalline Cu(II) compounds.[20] The relatively narrow "perpendicular" portion of the spectrum on the high-field side and the four-line hyperfine pattern (sometimes only three are resolved) associated with the higher g value and larger hyperfine splitting on the low-field side of the spectrum constitute the salient characteristics.

Typically, the $A_\parallel$ value is 140 G plus or minus about 20%. A routine examination of the upper portion of Figure 5 reveals an

(19) R. E. Coffman, *J. Chem. Phys.*, **48**, 609 (1968).

(20) B. J. Hathaway and D. E. Billing, *Coord. Chem. Rev.*, **5**, 143 (1970).

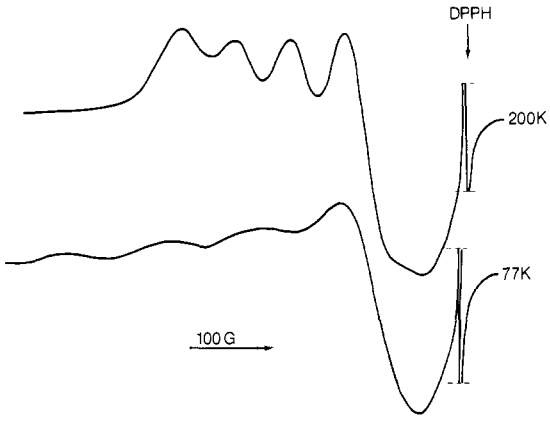

Figure 5. X-band EPR spectrum of $Cu_5(BTA)_6(t\text{-}C_4H_9NC)_4$ with the room-temperature form (upper spectrum) and the low-temperature form on the same scale.

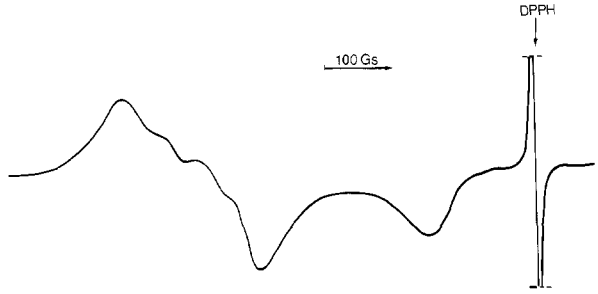

Figure 6. K-band EPR spectrum of $Cu_5(BTA)_6(t\text{-}C_4H_9NC)_4$ at room temperature.

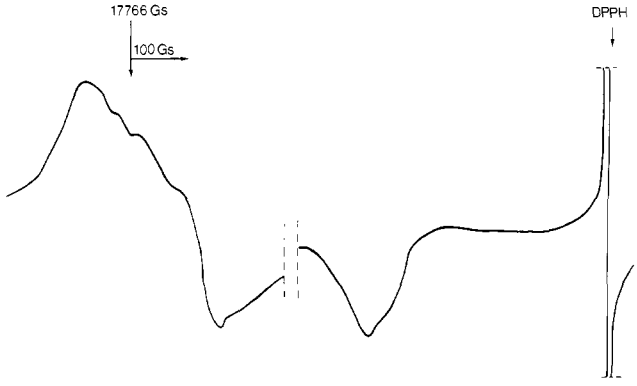

Figure 7. V-band spectrum of $Cu_5(BTA)_6(t\text{-}C_4H_9NC)_4$.

almost characteristic Cu(II) pattern. The $A_\parallel$ value is somewhat smaller than expected, and the "perpendicular" region is a bit broader, but the latter complication could be explained by the so-called "extra absorptions"[21] while the former might be associated with 4p orbital admixture.[20,21] Thus, the X-band high-temperature EPR spectrum does not appear to be unusual. The unique aspects do not become apparent until the higher frequency spectra are examined. The V- and K-band spectra of **1** are shown in Figures 6 and 7. The higher field portions of the spectrum have the appearance of a typical "parallel" peak while the lower field portions look almost isotropic although a closer examination shows that the center of the four-line pattern is above the base line. If we refer back to the upper portion of Figure 5, it is possible to see these aspects as well, but they are not clearly defined because of spectral overlap. The conclusion is that these three spectra, the upper one in Figure 5 and Figures 6 and 7, show a reversal in the usual "parallel" and "perpendicular" regions. The parallel

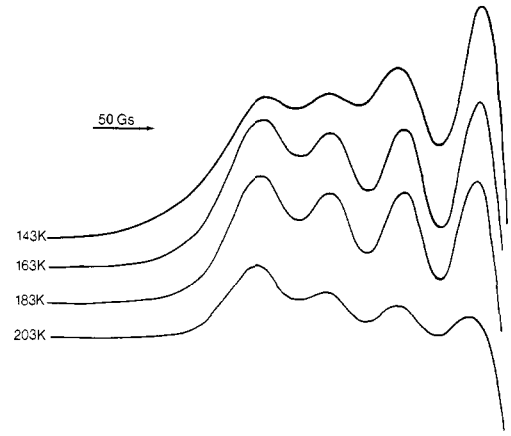

Figure 8. Temperature dependence of the parallel region of the EPR spectrum of $Cu_5(BTA)_6(t\text{-}C_4H_9NC)_4$.

(high field) g value in the high-temperature spectrum (upper trace in Figure 5) is just about equal to the perpendicular (high field) g value in the low-temperature spectrum (lower trace in Figure 5). On the other hand, the "perpendicular" (low field) g value in the high-temperature spectrum is the average of the perpendicular and parallel g values in the low-temperature spectrum. Furthermore, the value of the hyperfine splitting on the low-field side of the high-temperature spectra is just under one-half the value of that found in the low-temperature spectrum. This suggests an averaging of the g and A values:

$$g_\perp^{HT} = (g_\parallel^{LT} + g_\perp^{LT})/2$$

$$g_\parallel^{HT} = g_\perp^{LT}$$

$$A_\parallel^{HT} = (A_\parallel^{LT} + A_\perp^{LT})/2$$

$$A_\parallel L^T = A_\perp^{LT}$$

where HT and LT refer to values at high and low temperatures. In addition, it appears that the sign of $A_\perp^{LT}$ is opposite that of $A_\parallel^{LT}$ and that $A_\perp^{LT}$ is quite small (perhaps 10 G). The results are consistent with the two-dimensional Jahn–Teller effects described above, and indeed, this is the most reasonable way of accounting for such a reversal of spectral features. The usual mechanism for an apparent reversal of the parallel and perpendicular positions in the EPR of six-coordinate Cu(II) complexes is an exchange interaction.[2,20] This can be ruled out here because of the large Cu(II)–Cu(II) distance (vide supra) and because the observation of four hyperfine lines requires a value of J to be too small to produce g value averaging. The possibility of a d_{z^2} ground state is considered below.

The temperature-dependent effects might be expected to appear as a superposition of nonequivalent anisotropic spectra in proportion to their Boltzmann population. However, the vibrational relaxation has been found to be sufficiently rapid in all known cases so that only the average spectrum appears.[5] A gradual transition from the anisotropic to the isotropic spectrum is also expected with increasing temperature as the magnetic parameters are vibrationally averaged.

An important feature of this study is the clear evidence for the reduction of the vibrational motion with decreasing temperature, without the corresponding gradual transition of the g value above 128 K. As the amplitudes of lattice modes decrease with decreasing temperature, the clusters **1**, **2**, and **4** undergo a discontinuous change in line width in a process that we believe to be analogous to a phase transition (vide infra). In cluster **3**, however, typical three-dimensional Jahn–Teller effects were observed (vide infra). In pure molecular complexes, exchange and dipolar effects often obscure or modify major spectral characteristics.[22-25] In

(21) G. F. Kokoszka, C. W. Reimann, H. C. Allen, Jr., and G. Gordon, *Inorg. Chem.*, **6**, 1657 (1967).
(22) R. Wilson and D. Kivelson, *J. Chem. Phys.*, **44**, 154, 4440, 4445 (1966).
(23) R. H. Sands, *Phys. Rev.*, 99, 1222 (1955).
(24) A. Kwiatkowski, Z. Peplinski, and J. Baranowski, *Trans. Met. Chem.* **5**, 337 (1980), and references cited therein.

particular, the copper hyperfine structure is only infrequently resolved in these cases and, to our knowledge, never before in a pure compound exhibiting dynamical Jahn–Teller effects. In Figure 8, the dependence of line widths on M_I as a function of temperature is shown at X-band frequency.

At 203 K, there is the most complete averaging of the magnetic anisotropies that produces dependence on M_I and thus corresponds to the most complete vibronic activity. In sharp contrast (vide supra), the spectrum at 143 K shows the maximum variation in the hyperfine line width with M_I and therefore reflects the diminution of vibronic motions. Such effects have been observed in solutions and less frequently in magnetically diluted crystalline or glass samples.[21,23,25,26]

This behavior is analogous to "mode softenings" or Kohn anomaly found in one-dimensional conducting materials as the Peierls transition is approached.[27] The reduction or transformation of particular vibrational modes can be connected with a phase transition. Here, this phase transition cannot result in dramatic molecular rearrangements because of its reversible nature. Nevertheless, the major variations observed lead to the conclusion that $Cu_5(BTA)_6(t\text{-}C_4H_9NC)_4$ moieties are adjusting their local average environments in ways that do not affect the major magnetic parameters (g and A values) but rather are apparent from the more subtle line-width dependence.

In $Cu_5(BTA)_6(c\text{-}C_6H_{11}NC)_4$ (**2**) a similar effect was observed but the hyperfine lines are spaced somewhat closer (see Table IV), and the corresponding spectra are less clearly resolved. Furthermore, the phase-transition temperature is approximately 100 °C higher than that in $Cu_5(BTA)_6(t\text{-}C_4H_9NC)_4$. Nevertheless, the existence of the dynamical two-dimensional Jahn–Teller effect in both of these molecules, the general similarities in the matrix behavior, and the fact that both exhibit the sharp changes of spectral features in a narrow temperature range all suggest that the local environment at the Cu(II) site, which is our internal probe, is not significantly different in either the high- or low-temperature forms of these two molecules.

The sharp temperature-dependent behavior of the two compounds discussed above may be compared with the more usual case of a gradual spectral transformation as found in $Cu_5(BTA)_6(i\text{-}C_3H_7NC)_4$ (**3**). Here, the normal behavior for a Jahn–Teller compound is found. Over a range of about 200 °C, the spectrum undergoes a continuous transformation from the full anisotropic case to the isotropic situation. The line widths of the individual hyperfine components are quite broad at room temperature, resulting in a barely resolvable pattern. Still, the value of the isotropic hyperfine splitting is almost one-third that of $A_\parallel$ in the low-temperature form.

Discussion

Condensation of copper(I) thiophenoxide, benzotriazole, and an organic isocyanide provides a general route to the mixed-valence clusters $Cu_5(BTA)_6(RNC)_4$. At least some oxygen appears to be required, and the yield drops drastically if air is rigorously excluded. Thiophenol, identified by mass spectrometry, is an initial product, and it is likely associated with the formation of Cu(BTA)RNC. The isocyanide complexes appear to be unique among the Cu(BTA)(ligand) class (ligand = pyridine, Ph_3P, Ph_2PCH_3) in that further reactions ensue. The requirement for oxygen implies that some Cu(I) is converted into Cu(II), which acts as a template on which cluster growth proceeds. The synthetic method employed here may have broader generality.

Inspection of the geometry of the central copper–nitrogen cluster indicates that a variety of complexes of the type (metal A)(metal B)$_4$(BTA)$_6$ could be prepared in which tridentate BTA ligands bridge the octahedrally coordinated metal A and the surrounding tetrahedral array of metal B ions. As the complex is not required to be neutral, the valences of the metal ions may vary. The structure proposed by Marshall[28] contains a copper–nitrogen cluster in which copper(II) is substituted for copper(I); the structure may be viewed as a $Cu^{II}{}_5(BTA)_6{}^{4+}$ cation neutralized by four 2,4-pentanedionato(1−) anions. In addition, similar metal–nitrogen clusters might be prepared by using two different metal ions. It is conceivable that the symmetry of the resulting complex may be higher than the tetragonal symmetry found for $Cu_5(BTA)_6(t\text{-}C_4H_9NC)_4$.

If the central copper(II) ion (Cu2) were replaced by a metal ion that has six equivalent metal–nitrogen coordinate bonds, it is likely that the symmetry of the complex would be cubic with point symmetry $\bar{4}3m$. Thus, by changing the valences of the metal ions and by using metals other than copper, a broad class of new metal–nitrogen clusters may be accessible.

In the $Cu_5(BTA)_6(RNC)_4$ clusters, no long-wavelength intervalence charge-transfer bands are observed. We attribute this to the near-ideal geometries of the copper sites: octahedral for Cu(II) and tetrahedral for Cu(I). Given the rigidity of the copper–nitrogen cluster, one would expect the reorganization energy for Cu(I)—Cu(II) transitions to be quite large and that such processes are improbable.

The resolution of the copper hyperfine splitting, but not the nitrogen superhyperfine splitting, deserves attention. Nitrogen superhyperfine lines are often observed in Cu(II) complexes in magnetically dilute matrices, particularly in the parallel spectral region where the four in-plane ligands are equivalent or nearly so. In $Cu_5(BTA)_6(t\text{-}C_4H_9NC)_4$, the criterion for equivalence may not be expected to be fully achieved even at low temperature. However, there is a further consideration that is more important. The degree of magnetic dilution is largely determined by the effective random magnetic field set up by nearby nuclear magnetic moments or more distant electronic magnetic moments. The usual criterion for magnetic dilution is the reduction of the line broadening due to the electronic magnetic moments to less than that of the nuclear moments (often associated with unresolved hydrogen interactions). The nuclear moments usually produce a residual line width of about 5 G although selective isotropic replacement (deuterium for hydrogen) can effect further reductions. In $Cu_5(BTA)_6(t\text{-}C_4H_9NC)_4$, an estimate of the residual electronic line broadening can be made by using the Van Vleck isotropic average expression for the dipolar field. Such an approximation should be quite reasonable in this lattice geometry. The equation is

$$H_d = 4.72 \times 10^4[(S)(S+1)]^{1/2}(d/m)$$

where the last term is the density divided by the molecular weight of the paramagnetic unit. We find that the average dipolar line width due to all Cu(II)–Cu(II) interactions is about 42 G. This value is greater than the typical nuclear magnetic dipolar broadening and also greater than the typical nitrogen superhyperfine interaction (which is typically 10–15 G). On the other hand, it is significantly less than the value of $A_\parallel$ in the low-temperature spectra and less than $A_\parallel/2$. This accounts for the resolution of the copper(II) nuclear hyperfine interactions but no additional spectral features in Figure 8. In fact, examination of the spectral features at 143 K shows that a half-width at half-height of some 40 G plus some additional hyperfine or superhyperfine interactions can account for the observed half-width at half-height of some 80 G in the high-field spectral region and the just-resolved copper(II) hyperfine pattern in the low-field region.

If the line width is examined from a slightly different point of view, another estimate can be made. As a rule of thumb, we usually estimate that a nuclear magnetic moment situated at a distance of 1 Å from a measurement position produces a field of 5 G. In this case we are dealing with an electronic moment at a distance of 12.86 Å. The ratio of the magnetic moments causes the 5-G estimate to be scaled upward by about a factor of 2000, while the ratio of the cube of the distances causes a reduction by about 2000. This approximate cancellation means that the effective field can be estimated by multiplying 5 G by the number of nearest neighbors, 8. This produces a value of about 40 G, in

(25) M. Noack, G. F. Kokoszka, and G. Gordon, *J. Chem. Phys.*, **54**, 1342 (1971).
(26) W. B. Lewis and L. O. Morgan, *Trans. Met. Chem.*, **4**, 433 (1968).
(27) P. M. Chaikin, *Ann. N.Y. Acad. Sci.*, **313**, 128 (1978).
(28) J. H. Marshall, *Inorg. Chem.*, **17**, 3711 (1978).

sensible agreement with the estimate made above.

The possibility that the data presented might have an alternate interpretation should be explored. The crystallographic data reveal a compressed O_h geometry about the Cu(II) ion. This suggests that the d_{z^2} orbital could be the ground state and that the dynamical Jahn–Teller effect need not be invoked in order to explain the high-temperature results. If such a model is used, then the low-temperature transition would simply involve a change in the molecular geometry and in the ground state. If the d_{z^2} orbital contains the unpaired electron, then the axially symmetrical **g** tensor would have the values[29]

$$g_1 = 2$$

$$g_2 = g_3 = 2 - 6w$$

where w is the spin–orbit coupling constant divided by the crystal-field splitting (about 10 Dq). A typical value for w (and for u and v, vide infra) would be 0.02–0.04 when covalency is included and when ligand spin–orbital effects are neglected. The latter approximation should be reasonable for six nitrogens in the first coordination sphere. The overall shape of the EPR spectrum and the value of g_2 ($=g_3$) are consistent with this picture, but the value of $g_\perp$ is significantly greater than 2.00. This result means that a "pure" d_{z^2} wave function is not the orbital in which the unpaired electron resides. Perhaps the most reasonable way to modify the model to allow g_1 to deviate from 2.00 is to incorporate some $d_{x^2-y^2}$ character into the predominantly d_{z^2} ground state. This is not allowed in D_4h symmetry but can be explored as one possibility and, should it be useful, might lead to uncovering new effects. In this model the g-value equations become[29]

$$g_1 = 2.00 - 8u(\sin a)^2$$

$$g_2 = 2.00 - 2v(\sqrt{3}\cos a + \sin a)^2$$

$$g_3 = 2.00 - 2w(\sqrt{3}\cos a - \sin a)^2$$

where $(\sin a)^2$ is an indication of the extent of $d_{x^2-y^2}$ admixture. In order to account for the experimental value of g_1 over a typical range of values of u, v, and w, it is necessary that g_2 and g_3 be different. It is possible that such an effect might not be resolvable at X-band (9 GHz).[30] However, it would certainly be evident in V-band (54 GHz) spectra. There is no evidence in either of the two high-frequency spectra (see Figures 6 and 7) for any breakup of the perpendicular portion of the spectrum into two components.

Furthermore, if the ground state were d_{z^2}, a value of some 50 or 60 G for the Cu(II) hyperfine coupling would be expected about the high-field g value.[31] This four-line pattern should have been resolved in the high-frequency spectra or, at the very least, produce a flat-topped rather than peaked spectral shape. Again, the evidence seems to rule out d_{z^2} ground state.

Finally, a dynamical Jahn–Teller effect would be consistent with motional features in the spectra, while a d_{z^2} ground state might well exhibit mostly static line-shape features. The temperature-dependent line widths that are functions of the nuclear quantum number are most easily explained by the former model. Any one of the three pieces of evidence cited above could have provided only a reasonable case for the proposed model, but all three, taken together, seem to make it quite plausible.

Acknowledgment. Acknowledgment is made to the donors of the Petroleum Research Fund, administered by the American Chemical Society, for support of the research carried out at State University of New York, Plattsburgh (G.F.K., C.G., and J.O.). Part of this work is from a dissertation accepted by the Graduate School, The Catholic University of America (V.L.H.). We are grateful for support from the National Research Council–National Bureau of Standards Postdoctoral Research Associateship Program and the National Bureau of Standards Graduate Cooperative Education Program, to the SUNY–Wroclaw Exchange Program administered by the Office of International Studies, State University of New York at Stony Brook (J.B.), and to Drs. C. R. Hubbard, R. M. Doherty, K. Karlin, and D. Reinen for assistance and counsel.

Registry No. 1, 79079-30-4; **2**, 86146-89-6; **3**, 86162-05-2; **4**, 86146-90-9; copper(I) thiophenoxide, 1192-40-1.

Supplementary Material Available: Tables of anisotropic thermal parameters and observed and calculated structure factors (11 pages). Ordering information is given on any current masthead page.

(29) G. F. Kokoszka, H. C. Allen, Jr., and G. Gordon, *J. Chem. Phys.*, **42**, 3693 (1965).

(30) J. Pradilla-Sorzano and J. P. Fackler, Jr., *Inorg. Chem.*, **13**, 38 (1974).

(31) A. Bencini, I. Bertini, D. Gatteschi, and A. Scozzafava, *Inorg. Chem.*, **17**, 3194 (1978).